Tingshu Hu
Department of Electrical and Computer Engineering,
University of Massachusetts Lowell,
Lowell, MA 01854
e-mail: tingshu@gmail.com

Zongli Lin
Charels L. Brown Department of Electrical and Computer Engineering,
University of Virginia,
P.O. Box 400743,
Charlottesville, VA 22904-4743
e-mail: zl5y@virginia.edu

Wei Jiang
Department of Mechanical and Aerospace Engineering,
University of Virginia,
P.O. Box 400746,
Charlottesville, VA 22904-4743
e-mail: wj2b@virginia.edu

Paul E. Allaire
Department of Electrical and Aerospace Engineering,
University of Virginia,
P.O. Box 400746,
Charlottesville, VA 22904-4746
e-mail: pea@virginia.edu

Constrained Control Design for Magnetic Bearing Systems[1]

We study control problems in magnetic bearing systems that are subject to both input and state constraints. Apart from the usual restrictions on voltages and currents in the circuit systems, most magnetic bearing systems are subject to a severe state constraint: the motion of the rotor (the suspended object) is only allowed in an extremely small airgap, otherwise the collision of the rotor and the stator would cause severe damages. Traditional methods for avoiding a collision include increasing the airgap and increasing the currents, which would usually result in unnecessarily large capacity of power supply and power loss. In this paper we present a systematic approach for dealing with all the input and state constraints by using some recently developed tools for constrained control design. Issues on the stability region, robustness, disturbance rejections, and transient response are addressed. We hope that by dealing with the constraints properly, safety operation can be ensured with relatively small currents and power consumption. Experiments on the balance beam test rig in our laboratory show that the design techniques are effective. [DOI: 10.1115/1.2101850]

1 Introduction

Active magnetic bearings (AMB) have several appealing advantages over traditional bearings, such as very low power loss, very long life, the elimination of the oil supply, low weight, the reduction of a fire hazard, vibration control, and diagnostic capability [1]. They have been utilized in a variety of rotating machines, ranging from artificial heart pumps, compressors, high-speed milling spindles to flywheel energy storage systems (see, e.g., [2–7]). This work is intended to develop a systematic design approach to the control of magnetic bearing systems through a simple experimental setup at the University of Virginia. A key feature of our approach is that it takes state and control constraints into account in the design of feedback laws.

The experimental system we use in this paper is a beam balancing test rig (see Fig. 1 for a picture of the test rig and Fig. 2 for an illustrative diagram). It consists of a beam free to rotate on a pivot at its center of mass, and stabilized by electromagnets located at both ends of the beam. This experiment mimics the dynamics of a single axis AMB system. It captures the fundamental features of many magnetic bearing systems yet is quite simple from a mechanical viewpoint. Recently, in [8], we attempted to characterize the relationship between several performances and the biasing level through the numerical optimization method.

The dynamics of the beam can be modeled by the following differential equation (see, e.g., [9]):

$$J\ddot{\theta} = -D\dot{\theta} + T_2 - T_1, \tag{1}$$

where θ is the angle between the beam and the horizontal direction, and T_1 and T_2 are the torques generated by the two electromagnets. The total torque provided by the electromagnets is $T_2 - T_1 =: T$. The system parameters are J—moment of inertia and D—system damping due to air and pivot friction.

The two electromagnetic circuits are described by the following differential equations:

$$L_1\dot{I}_1 = v_1 - I_1\dot{L}_1 - R_1 I_1, \tag{2}$$

$$L_2\dot{I}_2 = v_2 - I_2\dot{L}_2 - R_2 I_2, \tag{3}$$

where

$$L_1 = \frac{L_0 g_0}{g_0 + \theta}, \quad L_2 = \frac{L_0 g_0}{g_0 - \theta},$$

L_0 is the inductance of the coil when the beam is balanced ($\theta = 0$) and g_0 is the maximal angle that is reached when one end of the beam touches an electromagnet. The torques are determined from the airgap fluxes in terms of I_1, I_2, and θ as follows,

$$T_1 = c_{t1}\left(\frac{g_0 I_1}{g_0 + \theta}\right)^2, \quad T_2 = c_{t2}\left(\frac{g_0 I_2}{g_0 - \theta}\right)^2,$$

where c_{t1} and c_{t2} are constants. In our test rig, $R_1 = R_2 = R$ and $c_{t1} = c_{t2} = c_t$.

Different magnetic bearing systems can be modeled similarly to the above balance beam system. For example, [10] considered a rotor whose one dimensional position was controlled by a pair of electromagnets. The model in [10] is mathematically the same as the one in this paper. Similar models were studied in [11,12], etc.

[1]Work completed at the University of Virginia and supported in part by NSF under grant CMS-0324329.

Contributed by the Dynamic Systems, Measurement, and Control Division of ASME for publication in the JOURNAL OF DYNAMIC SYSTEMS, MEASUREMENT, AND CONTROL. Manuscript received April 18, 2003; final manuscript received January 24, 2005. Associate Editor: Ranjan Mukherjee.

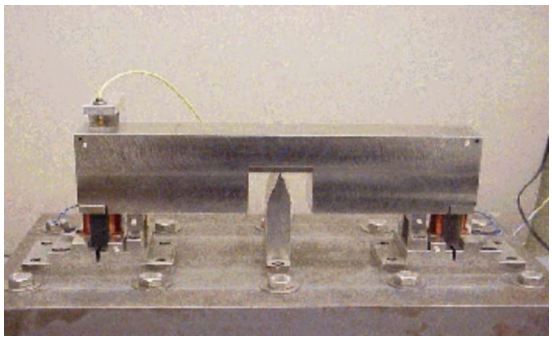

Fig. 1 The beam balancing test rig

More complicated magnetic bearings are usually composed of several pairs of electromagnets as modeled above.

The magnetic bearing system (1)–(3) is a control system subject to both input and state constraints. First, the voltage supplies are always bounded, so we have $|v_1|, |v_2| \leq v_M$, for some v_M. The relation between the bound on the voltages and the performances of magnetic bearings was studied in [13]. Second, the peak of the currents I_1 and I_2 is restricted to within certain bound I_M to prevent flux saturation, and the average of each current is restricted to prevent overheating (or excessive power loss). Note that the peak current also has an implementation constraint when the constant current sum scheme ($I_1 = I_0 + I, I_2 = I_0 - I$) is used. In this case, the control current I is subject to $|I| \leq I_0$ to ensure $I_1, I_2 \geq 0$. Finally but most importantly, the displacement θ must be kept within $|\theta| \leq g_0 - \varepsilon$ (for certain small number ε) to prevent the contact of the beam with the stator. The state constraints are often the most severe and must be observed. In rotational machinery suspended by magnetic bearings, the rotor usually spins at a very high speed and the collision of the rotor with the stator will cause severe damage to the whole system. A factor that makes the control design even more difficult is that the displacement of the rotor is restricted to an extremely small value due to the usually very small airgap.

It appears to us that these constraints in the magnetic bearing systems have not been addressed systematically in the literature and in the industry. Although the voltage bound and the current bound can be selected according to the required force slew rate, the load tolerance and other performance requirements through estimation, this selection could be conservative and could lead to an oversized power supply. Some efforts have been made toward dealing with the voltage bound and the current bound, for instance, in Refs. [14,15]. However, the state constraints, as far as we know, have not been paid sufficient attention. A common strategy is to restrict the motion of the rotor to a small portion of the airgap to avoid collision and to weaken the nonlinearity. This generally would result in an unnecessarily large airgap and hence unnecessarily large currents, since the electromagnetic force is proportional to the inverse of the distance. We hope that, by dealing with all these constraints properly, the rotor would be allowed to move in almost the full airgap without causing a collision and the currents and the capacity of power supply would be reduced considerably.

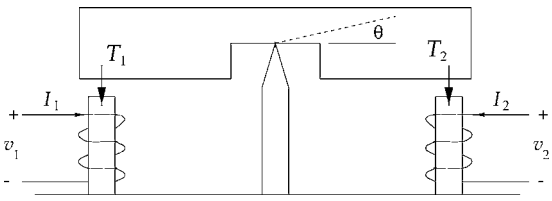

Fig. 2 An illustration diagram for the test rig

Recently, we developed a set of analysis and design tools to deal with input constraints (or actuator saturation) in control systems. These results are contained in the book [16] and some journal articles, e.g., [17,18]. In this paper, we will extend the results in [16–18] and develop some tools to deal with both input and state constraints in magnetic bearing systems. To use these tools, we need to obtain a linearized model. There are different ways to linearize a magnetic bearing system, including Jacobian linearization, feedback linearization, and other approaches (see, e.g., [12,19]). We first adopt the conventional Jacobian linearization approach and will explain through stability analysis why it only works well under a large bias current. We will then present an exact linearization approach based on a nonlinear current allocation strategy. We also present an almost linearization approach for the voltage mode. From our experience with the balance beam test rig, among these three linearization methods, the exact linearization approach appears to lead to the best results: full utilization of the airgap, small bias current, and robustness against parameter uncertainties.

The remainder of the paper is organized as follows. In Sec. 2, we present some design tools for linear systems with input and state constraints, including stabilization and performance improvement. In Sec. 3 we design controllers to enlarge the stability region through three linearization approaches. These three design approaches are compared through theoretical analysis and experimental verification. In Sec. 4 we address the issue of improving the transient performances. The effectiveness of the design techniques are also illustrated with experimental results. In Sec. 5 we conclude the paper.

Notation: For a real vector u, denote $|u|_\infty = \max_i |u_i|$. We use $\text{sat}: \mathbf{R}^m \to \mathbf{R}^m$ to denote the standard vector-valued saturation function, i.e., for $u \in \mathbf{R}^m$, the ith component of $\text{sat}(u)$ is $\text{sign}(u_i)\min\{1, |u_i|\}$.

2 Tools For Constrained Control Design

Virtually all control systems are subject to input saturation and state constraint. In a magnetic bearing system, the control inputs are voltages or currents. The voltage supplies are always bounded and the currents are restricted to within certain bounds to avoid flux saturation and overheating. The displacement of the suspended object is usually restricted to a very small value due to the usually small airgap. In this section, we develop some design tools to deal with the input and state constraints by extending some of the results in [16–18].

2.1 Systems With Input and State Constraints. Consider a linear system subject to input saturation and state constraint,

$$\dot{x} = Ax + Bu, \quad x \in \mathbf{R}^n, \quad u \in \mathbf{R}^m. \tag{4}$$

The input constraint is imposed as $|u|_\infty \leq 1$ and the state constraint is $x \in X_c$, where $X_c \subset \mathbf{R}^n$ is usually a polytope (a subset surrounded by hyperplanes) containing the origin in its interior. Our objective in this paper is to design a feedback law such that the closed-loop system possesses a large stability region and a good transient response. To design a feedback law such that the closed-loop system has a large stability region, we may construct a large invariant set, usually an invariant ellipsoid, that is inside the stability region.

An ellipsoid is associated with a positive definite matrix $P = P^{\mathrm{T}} \in R^{n \times n} (P > 0)$. Given a $P > 0$, define a Lyapunov function candidate as $V(x) = x^T P x$ and denote

$$\mathcal{E}(P) := \{x \in \mathbf{R}^n : x^T P x \leq 1\}.$$

We are interested in the control of system (4) by saturated linear feedback of the form $u = \text{sat}(Fx)$. The closed-loop system under this feedback law is

$$\dot{x} = Ax + B\,\text{sat}(Fx). \tag{5}$$

An ellipsoid $\mathcal{E}(P)$ is invariant for system (5) if and only if

$$\dot{V}(x) = 2x^{\mathrm{T}}P[Ax + B\,\mathrm{sat}(Fx)] \leqslant 0, \quad \forall\, x \in \partial\mathcal{E}(P).$$

In this case, all the trajectories starting from $\mathcal{E}(P)$ will stay inside it. If we further have

$$\dot{V}(x) = 2x^{\mathrm{T}}P[Ax + B\,\mathrm{sat}(Fx)] \leqslant -\beta x^{T}Px, \quad \forall\, x \in \mathcal{E}(P),$$

for some positive number β, then all the trajectories starting from $\mathcal{E}(P)$ will stay inside and converge to the origin. The number β can be considered as an indication of the convergence rate of the trajectories. A large β usually results in good transient performances: fast response and small overshoot.

For a matrix $F \in \mathbf{R}^{m\times n}$, let F_i be its ith row and denote

$$\mathcal{L}(F) := \{x \in \mathbf{R}^n : |F_i x| \leqslant 1, i = 1,2,\ldots,m\}.$$

We see that $\mathcal{L}(F)$ is a symmetric polytope, i.e., a subset of $\mathbf{R}^n$ surrounded by hyperplanes $F_i x = \pm 1$, $i = 1,2,\ldots,m$. If the feedback control is $u = \mathrm{sat}(Fx)$, then $\mathcal{L}(F)$ is the region where u is linear in x. For simplicity, we assume that the state constraint set is a symmetric polytope,

$$X_c = \mathcal{L}(G) = \{x \in \mathbf{R}^n : |G_i x| \leqslant 1, i = 1,2,\ldots,p\},$$

for some matrix $G \in \mathbf{R}^{p\times n}$. To ensure that the state constraint $x \in \mathcal{L}(G)$ is satisfied all the time, we can construct an invariant ellipsoid $\mathcal{E}(P)$ such that $\mathcal{E}(P) \subset \mathcal{L}(G)$.

2.2 Design For Large Stability Region. For any F such that $A+BF$ is Hurwitz, it is easy to see that the closed-loop system (5) is locally asymptotically stable. In the presence of a state constraint, the stability region is the set of initial conditions from which the state trajectories will stay inside $X_c = \mathcal{L}(G)$ and converge to the origin. One approach to enlarge the stability region is to design an F such that (5) has a large invariant ellipsoid inside $\mathcal{L}(G)$. The largeness of an ellipsoid can be measured with respect to a group of reference points $x_1, x_2, \ldots x_\ell$, by the number α_R defined as follows:

$$\alpha_R(P) := \max\{\alpha > 0 : \alpha x_i \in \mathcal{E}(P)\ \forall\, i\}.$$

For example, suppose that the state of the system in (1) is $x = [\theta\ \ \dot{\theta}]^T$ and we would like to achieve stabilization for a large initial angular displacement. We can then choose $x_1 = [1\ \ 0]^T$.

The problem of searching for an F that maximizes the invariant ellipsoid can be described as the following optimization problem

$$\sup_{P>0,F} \alpha \tag{6}$$

$$\text{s.t.} \quad (a) \quad \alpha x_i \in \mathcal{E}(P), i = 1,2,\ldots,\ell,$$

$$(b) \quad (A + BF)^{\mathrm{T}}P + P(A + BF) \leqslant -\beta P,$$

$$(c) \quad \mathcal{E}(P) \subset \mathcal{L}(F),$$

$$(d) \quad \mathcal{E}(P) \subset \mathcal{L}(G).$$

Under constraints (b) and (c), $\mathcal{E}(P)$ is an invariant ellipsoid. Constraint (d) guarantees that the state constraint is satisfied inside this ellipsoid. The number α in constraint (a) indicates the size of the ellipsoid. A positive β ensures a certain margin of stability.

The optimization problem (6) can be transformed into an LMI problem by using the tools developed in [17] (see also Chaps. 7 and 8 of [16]). Introducing new variables $Q = P^{-1}$, $H = FQ$, and $\gamma = 1/\alpha^2$, the optimization problem can be equivalently written as

$$\inf_{Q>0,H} \gamma \tag{7}$$

$$\text{s.t.} \quad (a) \quad \begin{bmatrix} \gamma & x_i^T \\ x_i & Q \end{bmatrix} \geqslant 0, \quad i = 1,2,\ldots,\ell,$$

$$(b) \quad QA^{\mathrm{T}} + AQ + H^{T}B + BH \leqslant -\beta Q,$$

$$(c) \quad \begin{bmatrix} 1 & h_j \\ h_j^{\mathrm{T}} & Q \end{bmatrix} \geqslant 0, \quad j = 1,2,\ldots,m,$$

$$(d) \quad g_k Q g_k^{\mathrm{T}} \leqslant 1, \quad k = 1,2,\ldots,p,$$

where h_j is the jth row of H and g_k is the kth row of G. The above problem can be solved efficiently with the LMI technique in [20]. For systems subject to external disturbances, we can use the methods in [18] to design a large invariant ellipsoid where a certain degree of disturbance rejection is achieved. There also exist other approaches to dealing with input and state constraints, for instance, in [21], where the control input is computed at each step by solving an LMI problem under the framework of model predictive control.

2.3 Design For Performance Improvement. As we will see in Example 2, Sec. 3.2, the controller designed by solving (6) may result in a slow transient response of the closed-loop system. To improve the transient response, we may try to maximize the number β in (b) of (6). Meanwhile, we would like to guarantee a certain desired stability region, for example, to ensure that the invariant ellipsoid $\mathcal{E}(P)$ include some desired points, $x_1, x_2, \ldots x_\ell$.

The problem of performance improvement with guaranteed stability region can thus be described by the following optimization problem:

$$\sup_{P>0,F} \beta \tag{8}$$

$$\text{s.t.} \quad (a) \quad x_i \in \mathcal{E}(P), \quad i = 1,2,\ldots,\ell,$$

$$(b) \quad (A + BF)^{T}P + P(A + BF) < -\beta P,$$

$$(c) \quad \mathcal{E}(P) \subset \mathcal{L}(F),$$

$$(d) \quad \mathcal{E}(P) \subset \mathcal{L}(G).$$

As in the treatment of the optimization problem (6), we let $Q = P^{-1}$ and $H = FQ$ to obtain an LMI problem:

$$\sup_{Q>0,H} \beta \tag{9}$$

$$\text{s.t.} \quad (a) \quad \begin{bmatrix} 1 & x_i^T \\ x_i & Q \end{bmatrix} \geqslant 0, \quad i = 1,2,\ldots,\ell,$$

$$(b) \quad QA^{\mathrm{T}} + AQ + H^{\mathrm{T}}B + BH \leqslant -\beta Q,$$

$$(c) \quad \begin{bmatrix} 1 & h_j \\ h_j^{T} & Q \end{bmatrix} \geqslant 0, \quad j = 1,2,\ldots,m,$$

$$(d) \quad g_k Q g_k^{\mathrm{T}} \leqslant 1, \quad k = 1,2,\ldots,p.$$

The constraint $\mathcal{E}(P) \subset \mathcal{L}(F)$ indicates that $|Fx|_\infty \leqslant 1$ and hence $\mathrm{sat}(Fx) = Fx$ for all $x \in \mathcal{E}(P)$, which means that the system (5) operates linearly inside the ellipsoid. Because of this, we have $|Fx|_\infty < 1$ for almost all $x \in \mathcal{E}(P)$. This means that the control input is almost always below the saturation level. To fully explore the control capacity, we may try to use a controller of the form

$$u = -\,\mathrm{sat}(kB^{T}Px). \tag{10}$$

Theoretically, by letting $k \to \infty$, the convergence rate of the Lyapunov function x^TPx is optimized (see Chap. 11 of [16]). However, all the practical systems have measurement noises, i.e., what we use for feedback is $x + \eta$ rather than the exact x, and the feedback control u is actually $u = -\mathrm{sat}[kB^{\mathrm{T}}P(x + \eta)]$. By increasing k, the effect of noises is also magnified, as we will see in Example 4, Sec. 4. If the noises are of high frequency and the state is close to the origin, excessively large k will cause the control to switch

between 1 and −1 constantly, causing an implementation issue. Hence it is important to choose a suitable k to achieve a desired convergence rate while keeping the effect of measurement noises acceptable.

2.4 Possible Reduction of the Actuator Capacity. By solving the optimization problem (6) or (8), we obtain an invariant ellipsoid $\mathcal{E}(P)\subset\mathcal{L}(G)\cap\mathcal{L}(F)$. The set inclusion relations $\mathcal{E}(P)\subset\mathcal{L}(G)$ and $\mathcal{E}(P)\subset\mathcal{L}(F)$ are generally not equally tight. This means that there may exist $\beta_G,\beta_F\in(0,1]$ such that $\mathcal{E}(P)\subset\beta_G\mathcal{L}(G)$ and $\mathcal{E}(P)\subset\beta_F\mathcal{L}(F)$. We maintain that at least one of β_G and β_F must be 1 by optimality. The reason is as follows. Suppose that (α,P,F) satisfy constraints (a)–(d). If both β_F and β_G are less that 1, then we can increase the size of the ellipsoid by a factor $\alpha_0>1$, such that $\alpha_0\mathcal{E}(P)\subset\mathcal{L}(G)$ and $\alpha_0\mathcal{E}(P)\subset\mathcal{L}(F)$, or, equivalently, $\mathcal{E}(P/\alpha_0^2)\subset\mathcal{L}(G)$ and $\mathcal{E}(P/\alpha_0^2)\subset\mathcal{L}(F)$. It is clear that if we replace P with P/α_0^2, the constraints (b), (c), and (d) are all satisfied. For constraint (a), it is still satisfied if α is replaced with $\alpha_0\alpha>\alpha$. In summary, $(\alpha_0\alpha,P/\alpha_0^2,F)$ will also satisfy constraints (a)–(d). This shows that if both β_F and β_G are less than 1, then (α,P,F) is not the optimal solution.

If $\beta_G<\beta_F=1$, then the input constraint is tighter. If $\beta_F<\beta_G=1$, then the state constraint is tighter, indicating that within the ellipsoid $\mathcal{E}(P)$, $|Fx|\leqslant\beta_F<1$, hence the actuator capacity can be reduced. In magnetic bearing systems, due to the extremely small airgap, we usually have a tighter state constraint than an input constraint. In that case, the size of the power supply can be reduced.

3 Stabilization

To use the design tools in Sec. 2, we need to obtain a linear model of the magnetic bearing system. There are different approaches to linearization. Beside the conventional Jacobian linearization, feedback linearization and other approaches have been developed recently [12,19]. In this section, we will present three linearization approaches and the corresponding constrained control designs.

3.1 The Jacobian Linearization Under the Current Mode. The dynamics of the beam balancing test rig under the current mode can be modeled by the following differential equation,

$$J\ddot{\theta}=-D\dot{\theta}+c_t\left[\left(\frac{g_0I_2}{g_0-\theta}\right)^2-\left(\frac{g_0I_1}{g_0+\theta}\right)^2\right],\tag{11}$$

where J,D,c_t, and g_0 are constants and g_0 is the maximal angular displacement that is reached when the beam touches one of the electromagnets. So we have $|\theta|\leqslant g_0$. It is assumed that $|I_1|,|I_2|\leqslant I_M$ to avoid flux saturation and overheating of the coils.

In the current mode, a circuit feedback law has been designed such that the actual current will closely follow a reference signal. We assume that the circuit dynamics can be ignored and the difference between the actual I_1 and I_2 and the desired I_1 and I_2 is sufficiently small. In this case, we consider I_1 and I_2 as the control inputs.

3.1.1 The Linearized Model and the Feedback Law. In (11), the currents appear in the form of I_1^2 and I_2^2, which are highly nonlinear for a control system. A conventional way to reduce this nonlinearity is to introduce a bias current $I_b>0$ and let I_1 and I_2 operate symmetrically around I_b, i.e.,

$$I_1=I_b+I,\quad I_2=I_b-I,\tag{12}$$

where I is considered as a control input that produces a net torque on the beam. Because of the bounds on the currents, we impose the constraint $|I|\leqslant I_M-I_b$ for simplicity. It should be noted that this constraint is more conservative than the original constraint $|I_1|,|I_2|\leqslant I_M$.

With I_1 and I_2 determined from (12), the dynamical relation between the input I and the output θ is,

$$J\ddot{\theta}=-D\dot{\theta}+c_t\left[\left(\frac{g_0(I_b-I)}{g_0-\theta}\right)^2-\left(\frac{g_0(I_b+I)}{g_0+\theta}\right)^2\right],\tag{13}$$

which is still a nonlinear system. Performing Jacobian linearization at $(\theta,\dot{\theta})=(0,0)$ and $I=0$, we obtain

$$\begin{bmatrix}\dot{\theta}\\ \ddot{\theta}\end{bmatrix}=\begin{bmatrix}0 & 1\\ \dfrac{4c_tI_b^2}{Jg_0} & -\dfrac{D}{J}\end{bmatrix}\begin{bmatrix}\theta\\ \dot{\theta}\end{bmatrix}+\begin{bmatrix}0\\ -\dfrac{4c_tI_b}{J}\end{bmatrix}I.\tag{14}$$

Denoting $x=[\theta\ \ \dot{\theta}]^T$ and

$$A_L=\begin{bmatrix}0 & 1\\ \dfrac{4c_tI_b^2}{Jg_0} & -\dfrac{D}{J}\end{bmatrix},\quad B_L=\begin{bmatrix}0\\ \dfrac{-4c_tI_b}{J}\end{bmatrix},$$

we obtain the linearized system

$$\dot{x}=A_Lx+B_LI,\quad |I|\leqslant I_M-I_b.\tag{15}$$

We notice that the open-loop linearized system (15) has an unstable pole since $\det(A_L)<0$.

Usually, a saturated linear feedback law $I=(I_M-I_b)\mathrm{sat}(Fx)$ is adopted, with F being designed based on the linearized model. The linearized closed-loop system is then given by

$$\dot{x}=A_Lx+B_L(I_M-I_b)\mathrm{sat}(Fx).\tag{16}$$

Under the feedback law $I=(I_M-I_b)\mathrm{sat}(Fx)$, the actual nonlinear closed-loop system is

$$J\ddot{\theta}=-D\dot{\theta}+c_t\left[\left(\frac{g_0[I_b-(I_M-I_b)\mathrm{sat}(Fx)]}{g_0-\theta}\right)^2-\left(\frac{g_0[I_b+(I_M-I_b)\mathrm{sat}(Fx)]}{g_0+\theta}\right)^2\right].\tag{17}$$

Based on the linearized model (15), we use the method in Sec. 2.2 to design an F for enlarging the stability region. In the optimization problem (6), we may choose $\ell=1$ and $x_1=(1,0)$. By solving (6), we will maximize the initial displacement of the beam that can be brought to the balance position. However, this only guarantees the stability of the linearized system (16). In what follows, we will examine how well the behavior of the linearized system (16) predicts that of the nonlinear system (17). By doing so, we will obtain some quantitative measure of the effect of the biasing current on the difference between the linearized model and the original nonlinear system.

3.1.2 Stability Analysis. The linearized model approximates the nonlinear system (13) very well when θ is close to zero. When θ is close to g_0, the nonlinearity gets stronger and usually causes the beam to hit one of the electromagnets and stay there. Experimental experience shows that for large I_b, it is easy to find an initial position such that the beam will be balanced by the controller. If I_b is too small, it is very hard to manipulate the beam (by hand) into a proper position so that it can be balanced by the controller. In what follows, we would like to explain this through a stability analysis of the linearized closed-loop system (16) and the actual closed-loop system (17).

Example 1. The parameters of the balance beam test rig are:

$$J=0.0948\ \text{kg m}^2,\quad g_0=0.004\ \text{rad},\quad c_t=0.1384\ \text{Nm/A}^2.$$

Since the damping parameter D is very small, we assume that it is 0. We choose $I_M=1$ A and use the method in Sec. 2.2 to design feedback laws. We take $A=A_L$, $B=B_L(I_M-I_b)$, where B absorbs the actual bound on the input I. The state constraint $|\theta|\leqslant 0.004$ is equivalent to $x\in\mathcal{L}(G)$ with $G=[1/0.004\quad 0]$. The controller will

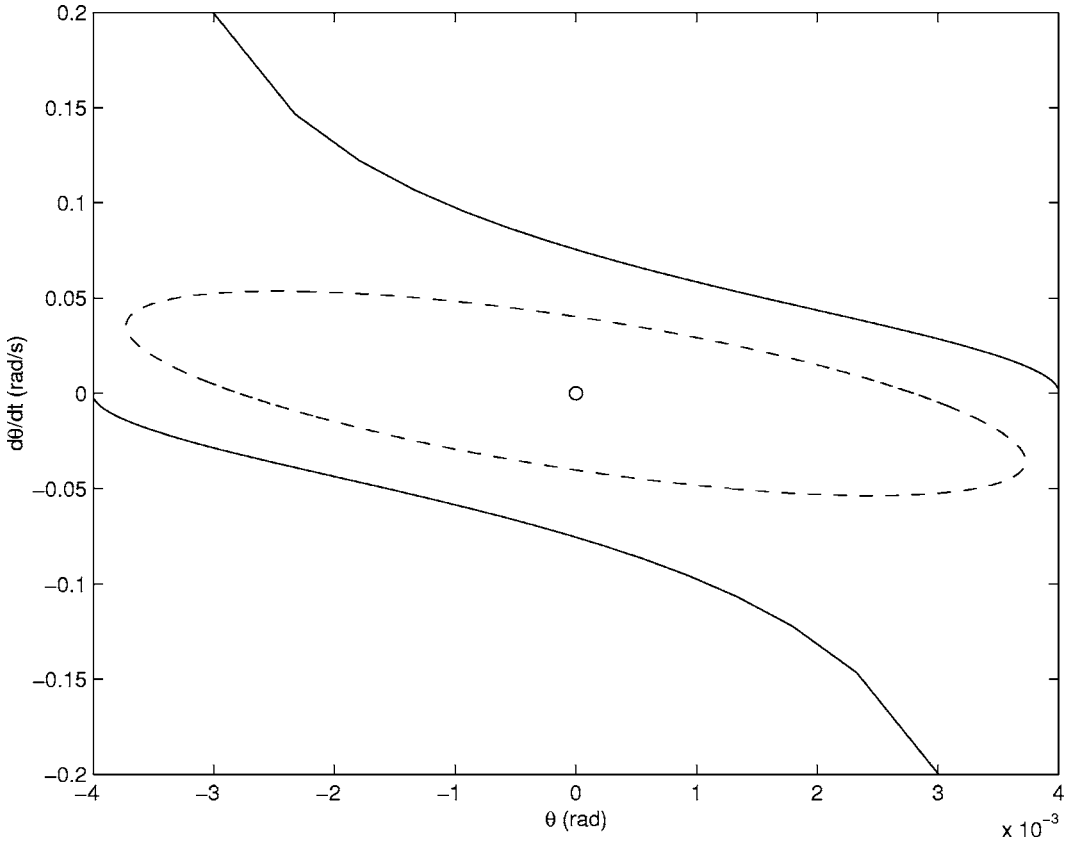

Fig. 3 The stability region under I_b=0.5 A and a valid estimate

be of the form $I=(I_M-I_b)\text{sat}(Fx)$. In solving (6), we set $\ell=1$ and choose $x_1=(1,0)$. To ensure certain stability margin, we choose $\beta=0.01$. We designed feedback laws for $I_b=0.5$ A and $I_b=0.1$ A. The actual stability region of the nonlinear closed-loop system (17) can be computed by the numerical method, for example, by simulating the time responses under different initial conditions.

For $I_b=0.5$ A, the optimal solution to (6) is $\alpha=0.0028$. The control law is

$$I = 0.5\ \text{sat}(357.7337\theta + 16.4353\dot{\theta}),$$

and the invariant ellipsoid is $\mathcal{E}(P)$ with

$$P = 10^5 \times \begin{bmatrix} 1.2797 & 0.0588 \\ 0.0588 & 0.0062 \end{bmatrix}.$$

Figure 3 plots the boundary of the estimated stability region of the linearized closed-loop system (16) in a dashed curve [the boundary of $\mathcal{E}(P)$] and the boundary of the actual stability region of the nonlinear closed-loop system (17) in solid curves. We see that the estimated stability region based on the linearized model is well inside the actual stability region of the nonlinear system and is a valid (though conservative) estimate.

For $I_b=0.1$ A, the optimal solution to (6) is $\alpha=0.004$. Notice that $g_0=0.004$ rad. This means that the beam should be balanced from the initial position where it touches one of the electromagnets. The control law is

$$I = 0.9\ \text{sat}(172.4701\theta + 9.8791\dot{\theta}),$$

and the invariant ellipsoid is $\mathcal{E}(P)$ with

$$P = 10^4 \times \begin{bmatrix} 6.2501 & 0.0016 \\ 0.0016 & 0.0859 \end{bmatrix}.$$

Figure 4 plots the boundary of the estimated stability region of the linearized closed-loop system (16) in a dashed curve and the boundary of the actual stability region of the nonlinear closed-loop system (17) in solid curves. In contrast to the case where $I_b=0.5$ A, most of the estimated stability region is outside the actual stability region. This means that most initial conditions will lead to unstable responses even if we predict stable responses based on the linearized model. For example, the beam will not be balanced by the controller if it is initially in touch with the electromagnets, as is verified by the experiment.

For comparison, we plot the boundary of the actual stability regions under $I_b=0.1$ A (in solid curves) and that under $I_b=0.5$ A (in dash-dotted curves) in Fig. 5. This explains why it is easier to balance the beam with a larger bias current. In the experiment, with $I_b=0.5$ A, the beam will be balanced even if it is initially in touch with one of the electromagnets. However, with $I_b=0.1$ A, it is very hard to manipulate the beam into an initial condition that can be balanced.

The above example shows that the relation between the estimated stability region of the linearized closed-loop system (16) and the actual stability region of the nonlinear closed-loop system (17) is quite complicated. The estimated stability region could be a subset of the actual stability region for large I_b. However, for small I_b, this relation does not hold. Because of this, it is hard to achieve a large stability region by designing the stabilizing feedback law based on Jacobian linearization, especially when the bias current is small.

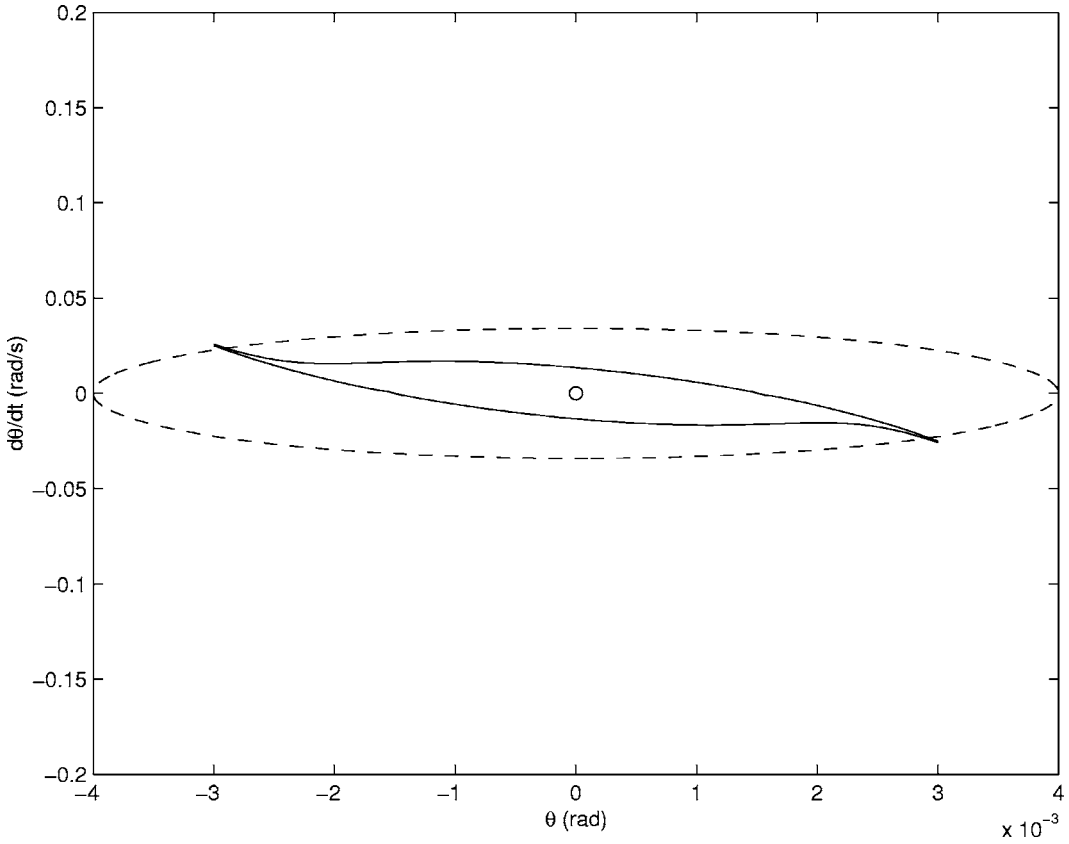

Fig. 4 The stability region under I_b=0.1 A and an invalid estimate

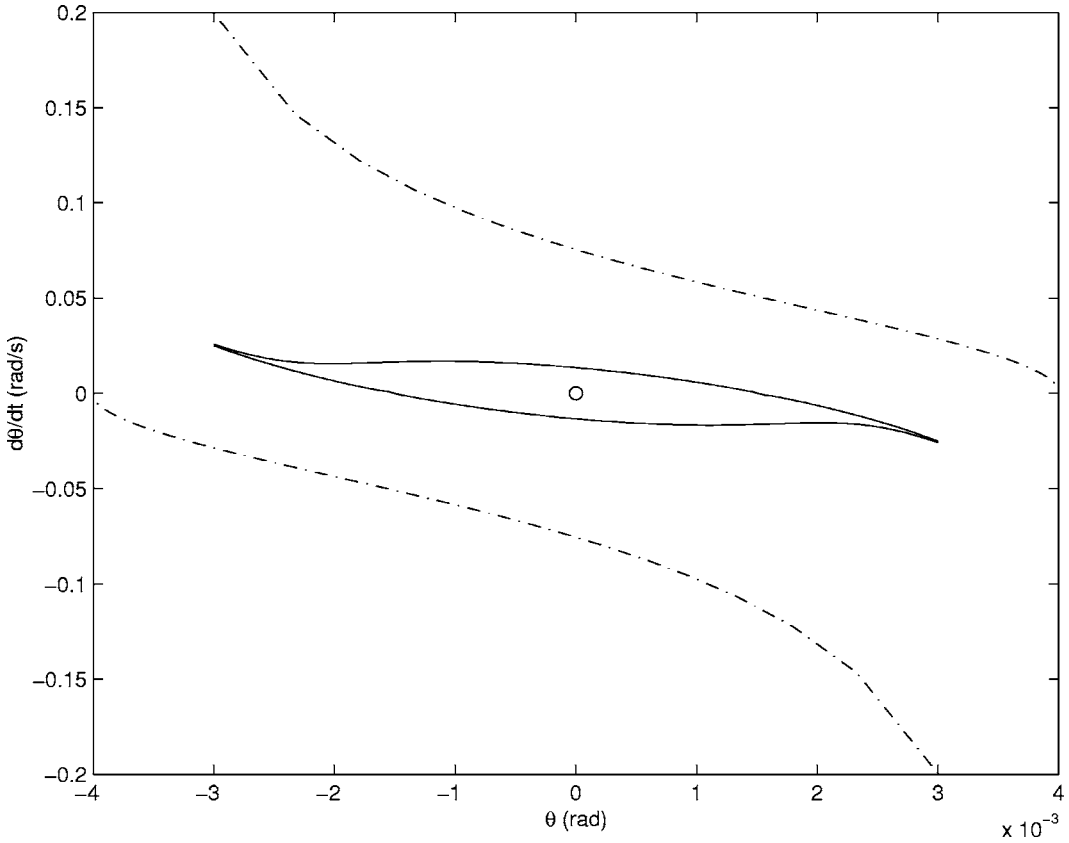

Fig. 5 The stability regions under I_b=0.1 A and 0.5 A

3.2 Exact Linearization Through Nonlinear Current Allocation. The simple linear relation between I_1, I_2, and I in (12) results in a nonlinear dynamical relation (13) between I and θ. This makes it hard to design a stabilizing controller for small bias current. In this section, we use the following nonlinear current allocation strategy,

$$I_1 = (I_b + I)\frac{g_0 + \theta}{g_0}, \quad I_2 = (I_b - I)\frac{g_0 - \theta}{g_0}. \tag{18}$$

Under this nonlinear current allocation, we have

$$\left(\frac{g_0 I_2}{g_0 - \theta}\right)^2 - \left(\frac{g_0 I_1}{g_0 + \theta}\right)^2 = (I_b - I)^2 - (I_b + I)^2 = -4 I_b I.$$

Hence, the dynamical relation between I and θ is exactly linear:

$$J\ddot{\theta} = -D\dot{\theta} - 4c_t I_b I, \tag{19}$$

or,

$$\begin{bmatrix} \dot{\theta} \\ \ddot{\theta} \end{bmatrix} = \begin{bmatrix} 0 & 1 \\ 0 & -\dfrac{D}{J} \end{bmatrix} \begin{bmatrix} \theta \\ \dot{\theta} \end{bmatrix} + I_b \begin{bmatrix} 0 \\ -\dfrac{4c_t}{J} \end{bmatrix} I.$$

Denoting

$$A_E = \begin{bmatrix} 0 & 1 \\ 0 & -\dfrac{D}{J} \end{bmatrix}, \quad B_E = \begin{bmatrix} 0 \\ -\dfrac{4c_t I_b}{J} \end{bmatrix},$$

we have

$$\dot{x} = A_E x + B_E I, \quad |I| \leq I_M/2 - I_b, \tag{20}$$

where the bound on I is imposed to guarantee that $|I_1|, |I_2| \leq I_M$. We also note that there is no problem in generating the currents given by (18) since the values of $(g_0 \pm \theta)/g_0$ are between 0 and 2 ($|\theta| \leq g_0$).

The system (20) is not only linear but also marginally stable with one open-loop pole at 0 and another one at $-D/J$.

In this section, we consider the problem of stabilizing system (20) in the presence of state and input constraints. The performance issue will be addressed in Sec. 4.

Let the feedback law be of the form

$$I = (I_M/2 - I_b)\text{sat}(Fx); \tag{21}$$

then the closed-loop system is

$$\dot{x} = A_E x + B_E(I_M/2 - I_b)\text{sat}(Fx). \tag{22}$$

We also use the method in Sec. 2.2 to find a large invariant ellipsoid $\mathcal{E}(P)$ by solving (6) with $A = A_E$, $B = B_E(I_M/2 - I_b)$, $x_1 = (1,0)$, and $\beta = 0.01$. Different from the design result in Sec. 3.1 for Jacobian linearization, in the case of exact linearization, $\mathcal{E}(P)$ is always inside the actual stability region. In what follows, we use an example to compare the invariant ellipsoid $\mathcal{E}(P)$ and the actual stability region. It turns out that $\mathcal{E}(P)$ is a good estimate of the actual stability region. Unlike the situation with the Jacobian linearization, where $\mathcal{E}(P)$ could be an overestimate of the actual stability region, here the linearization is exact and $\mathcal{E}(P)$ is always inside the actual stability region.

Example 2. Consider the same experimental system as in Example 1. Here we take $I_M = 2$ A. For $I_b = 0.5$ A, the optimal solution is $\alpha = 0.004$ and the controller is

$$I = 0.5\ \text{sat}(179.9578\theta + 6.2261\dot{\theta}).$$

The invariant ellipsoid is $\mathcal{E}(P)$ with

$$P = 10^4 \times \begin{bmatrix} 6.2502 & 0.0010 \\ 0.0010 & 0.0238 \end{bmatrix}.$$

Figure 6 plots the boundary of $\mathcal{E}(P)$, the estimated stability region, in a dashed curve and the boundary of the actual stability region in a solid curve.

For $I_b = 0.1$ A, the optimal solution is also $\alpha = 0.004$ and the controller is

$$I = 0.9\ \text{sat}(180.3603\theta + 10.3037\dot{\theta}). \tag{23}$$

The invariant ellipsoid is $\mathcal{E}(P)$ with

$$P = 10^4 \times \begin{bmatrix} 6.2502 & 0.0018 \\ 0.0018 & 0.0649 \end{bmatrix}.$$

Figure 7 plots the boundary of $\mathcal{E}(P)$ in dashed curve and the boundary of the actual stability region in a solid curve.

It should be noted that the stability regions are generated from the mathematical models. Since the difference between the model and the real system is unavoidable, it is expected that the stability regions for the real systems are different from those plotted in Figs. 6 and 7. Here we would like to use some experimental results to show that our stability analysis on the models gives a good estimation of the behavior of the actual system.

From Fig. 7, we see that the beam can be stabilized from initially touching the electromagnets, even with $I_b = 0.1$ A. This result was verified experimentally. The plots in Fig. 8 are the time responses under a bias current $I_b = 0.5$ A and the plots in Fig. 9 are the time responses under $I_b = 0.1$ A, all obtained from experimental data. The first plots in Figs. 8 and 9 are the time responses of the beam angle. The second and the third plots are the time responses of the currents I_1 and I_2. They were produced by pushing the beam to touch one of the electromagnets and then letting it go. After the steady state had been reached, the beam was pushed to touch the other electromagnet. This procedure was repeated several times for each set of the plots. As we can see, the beam always went back to the balance position. This was impossible with a bias current $I_b = 0.1$ A under the controller based on the Jacobian linearization (14).

Experimental experience shows that the system is very robust against parameter uncertainties and disturbances, even with $I_b = 0.1$ A. For example, we incorporated uncertain gains k_1 and k_2, and some drifts in the actuators so that the currents were

$$I_1 = k_1(I_b + I)\frac{g_0 + \theta}{g_0} + I_{10}, \quad I_2 = k_2(I_b - I)\frac{g_0 - \theta}{g_0} + I_{20}. \tag{24}$$

We tried with $(k_1, k_2, I_{10}, I_{20}) = (1, 1, -0.028, 0.05)$ and $(k_1, k_2, I_{10}, I_{20}) = (0.8, 1.2, 0, 0)$, respectively. The time responses of the beam angle are shown in Fig. 10, where the first plot corresponds to $(k_1, k_2, I_{10}, I_{20}) = (1, 1, -0.028, 0.05)$ and the second corresponds to $(k_1, k_2, I_{10}, I_{20}) = (0.8, 1.2, 0, 0)$. We see that stability is maintained under these parameter changes. The transient performances are slightly different. The overshoot from one side is larger than that from the other side.

3.3 The Voltage Mode: Almost Linearization. In the voltage mode, the currents are determined by the voltages in the circuit systems

$$L_1\dot{I}_1 = v_1 - I_1\dot{L}_1 - RI_1, \tag{25}$$

$$L_2\dot{I}_2 = v_2 - I_2\dot{L}_2 - RI_1, \tag{26}$$

where

$$L_1 = \frac{g_0}{g_0 + \theta}L_0, \quad L_2 = \frac{g_0}{g_0 - \theta}L_0.$$

In this section, we investigate the control design in the voltage mode, where the inputs are v_1 and v_2.

To deal with the nonlinearity in the system, we define some new input and state variables. Let

$$u_1 = v_1 - RI_1, \quad u_2 = v_2 - RI_2,$$

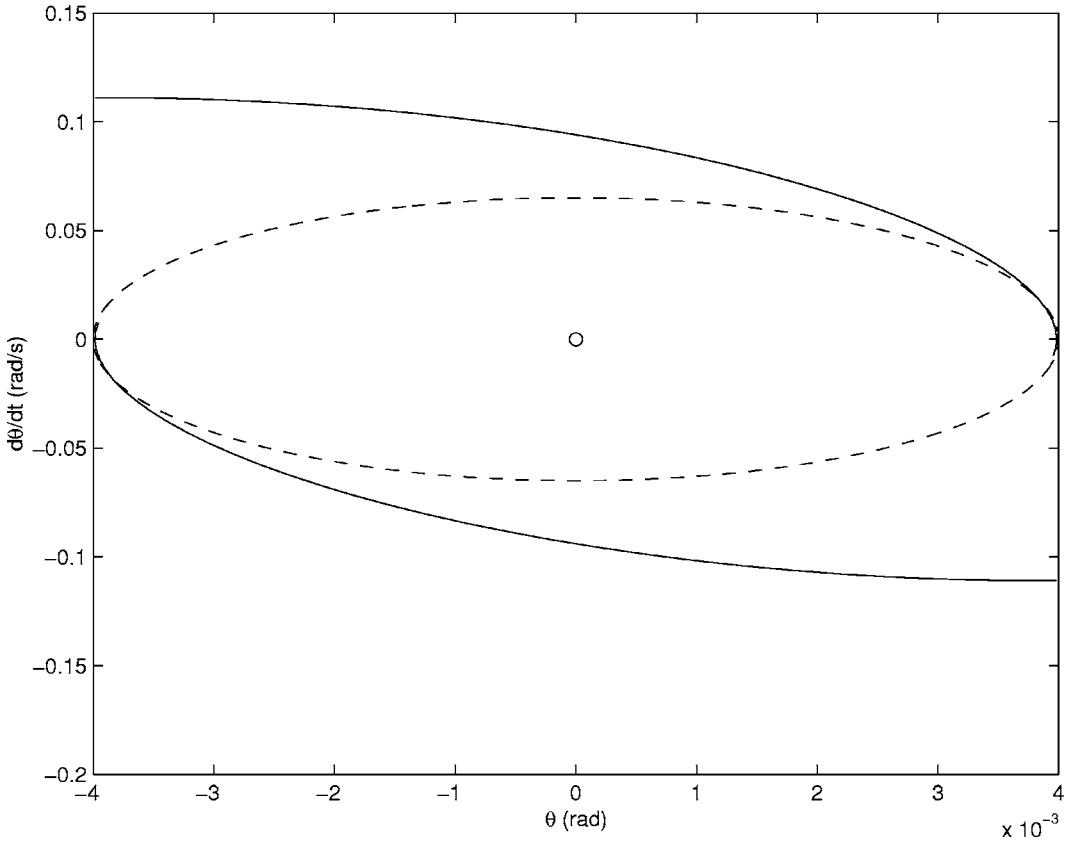

Fig. 6 The estimated stability region and the actual stability region: I_b=0.5 A

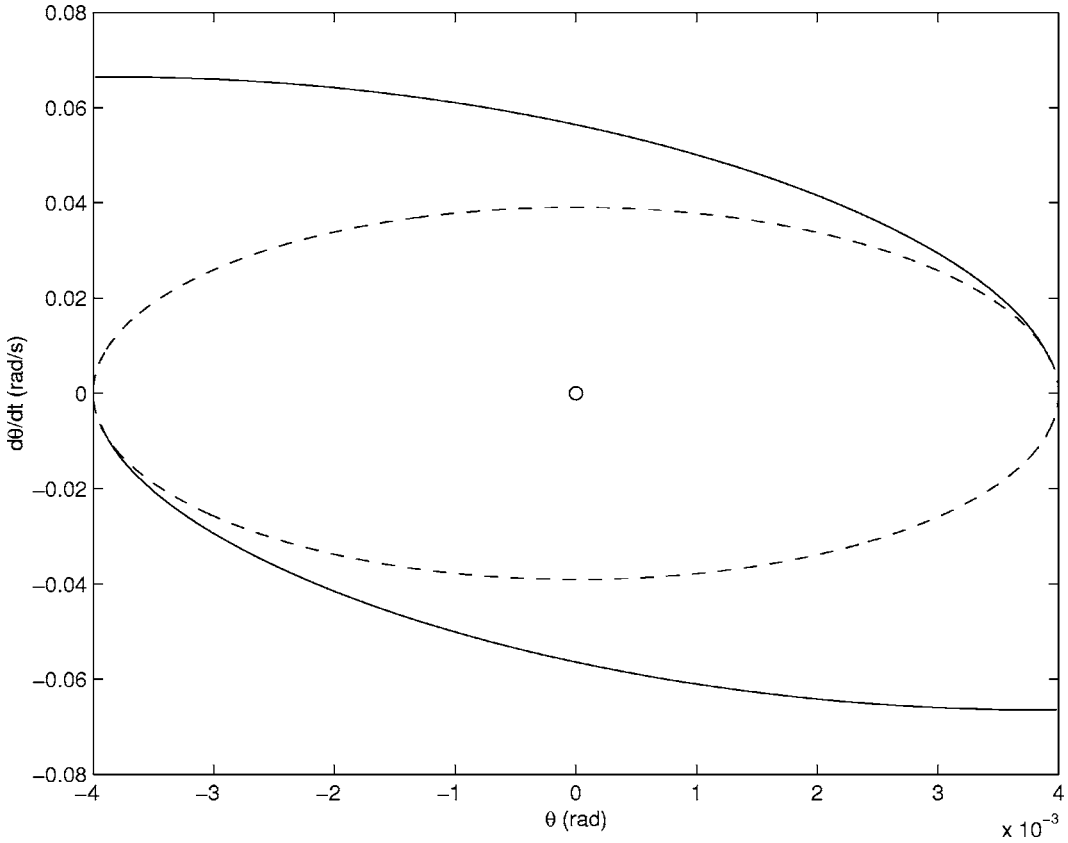

Fig. 7 The estimated stability region and the actual stability region: I_b=0.1 A

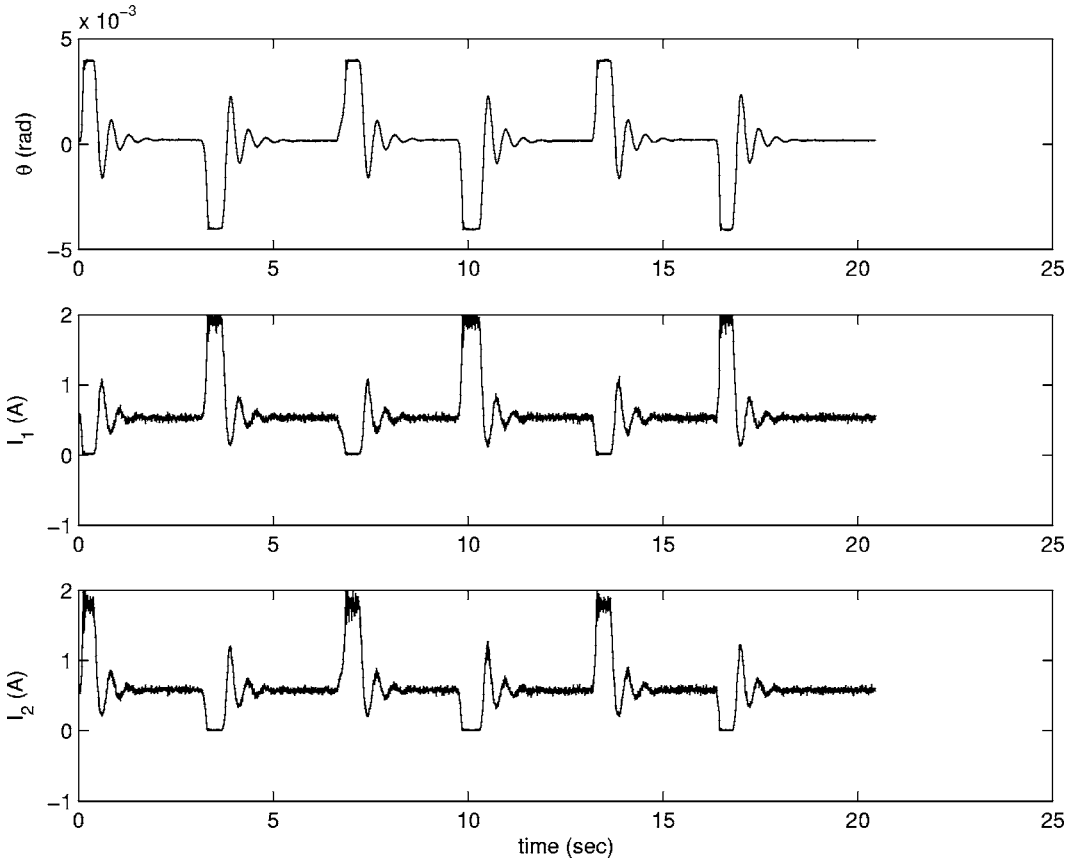

Fig. 8 Experimental results: time responses of θ, I_1, and I_2 under I_b=0.5 A

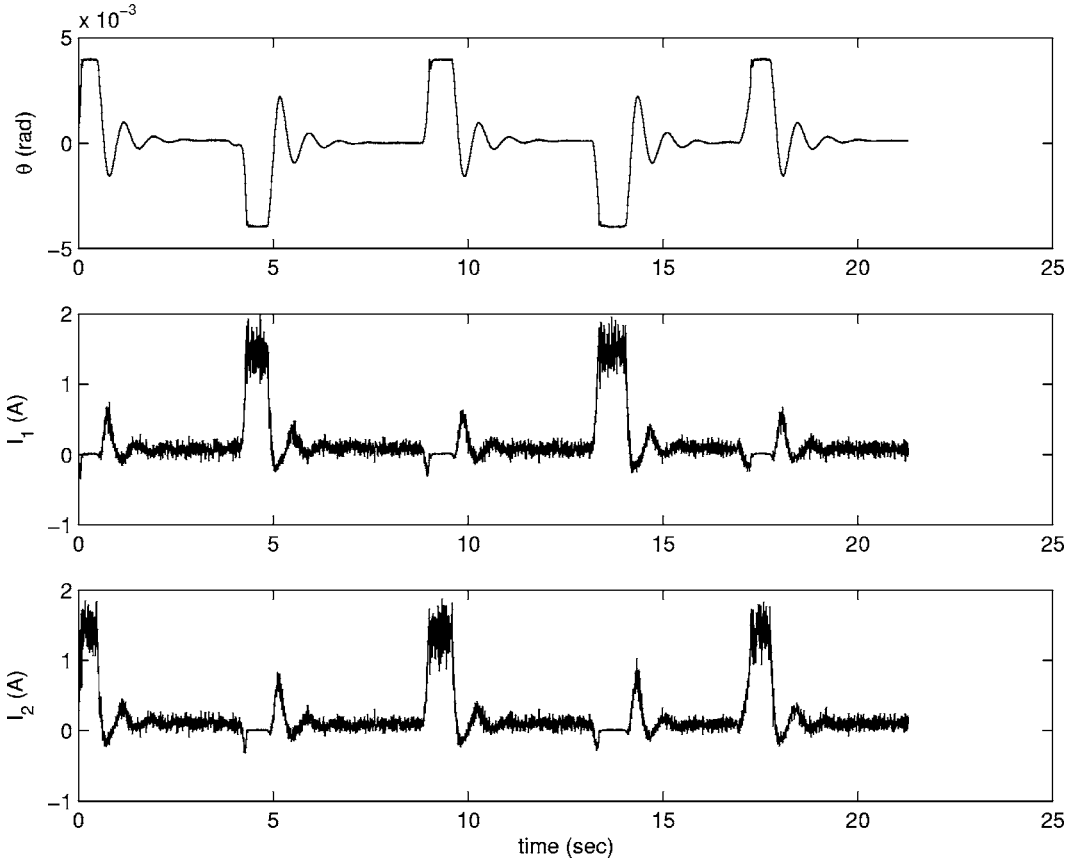

Fig. 9 Experimental results: time responses of θ, I_1, and I_2 under I_b=0.1 A

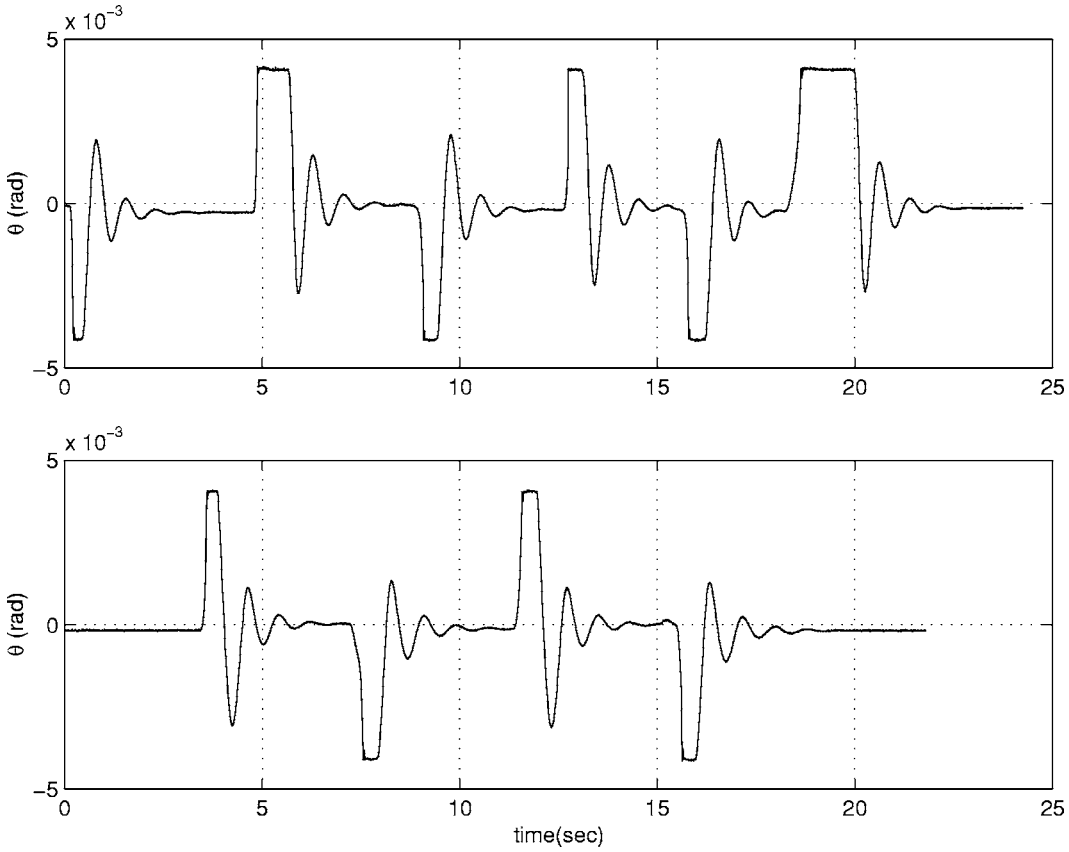

Fig. 10 Experimental results: time responses of θ under parameter changes for I_b=0.1 A

$$\phi_1 = \frac{g_0}{g_0+\theta} L_0 I_1, \quad \phi_2 = \frac{g_0}{g_0-\theta} L_0 I_2.$$

Then we have

$$\ddot{\theta} = -\frac{D}{J}\dot{\theta} + \frac{c_t}{JL_0^2}(\phi_2^2 - \phi_1^2), \tag{27}$$

$$\dot{\phi}_1 = u_1, \tag{28}$$

$$\dot{\phi}_2 = u_2. \tag{29}$$

In fact, ϕ_1 and ϕ_2 are the fluxes in the electromagnets. If we further define $\phi_b=(\phi_1+\phi_2)/2$, $\phi=(\phi_2-\phi_1)/2$, $w_1=(u_2-u_1)/2$ and $w_2=(u_1+u_2)/2$, we obtain

$$\ddot{\theta} = -\frac{D}{J}\dot{\theta} + \frac{4c_t}{JL_0^2}\phi_b\phi, \tag{30}$$

$$\dot{\phi} = w_1, \tag{31}$$

$$\dot{\phi}_b = w_2. \tag{32}$$

Notice that there is a bilinear term $\phi_b\phi$ in (30). Since ϕ_b is under the control of the input w_2 and is independent of other states, we can use a simple controller,

$$w_2 = k_1(\phi_{bd} - \phi_b), \tag{33}$$

with a positive number k_1 to make ϕ_b approximate some constant ϕ_{bd}. After ϕ_b has reached a steady state, the other states θ, $\dot{\theta}$, and ϕ and the input w_2 satisfy the following linear relation

$$\begin{bmatrix} \dot{\theta} \\ \ddot{\theta} \\ \dot{\phi} \end{bmatrix} = \begin{bmatrix} 0 & 1 & 0 \\ -\frac{D}{J} & 0 & \frac{4c_t}{JL_0^2}\phi_b \\ 0 & 0 & 0 \end{bmatrix} \begin{bmatrix} \theta \\ \dot{\theta} \\ \phi \end{bmatrix} + \begin{bmatrix} 0 \\ 0 \\ 1 \end{bmatrix} w_1. \tag{34}$$

For the above system, a simple linear feedback law of the form

$$w_1 = k_2\theta + k_3\dot{\theta} + k_4\phi \tag{35}$$

can be designed to meet certain performance and stability requirements.

The closed-loop system (30)–(33) and (35) is not strictly linear because of the bilinear term $\phi_b\phi$. The transient dynamics of ϕ_b can be considered as a disturbance, $(4c_t/JL_0^2)(\phi_b-\phi_{bd})\phi$, whose energy is finite and can be adjusted by the design parameter k_1. If the control law (35) has a certain degree of robustness and if the dynamics of ϕ_b is fast, then the performances of the whole system will be close to those of the linear system (34) and (35).

It should be noted that the idea of obtaining a linear system by setting the sum of the fluxes fixed is similar to that in [12]. Different from [12], here we take the voltages as inputs and the dynamics of the fluxes is considered. Moreover, we will also address all the input and state constraints in our design.

From the feedback laws (33) and (35), the feedback relation between the original states $(\theta, \dot{\theta}, I_1, I_2)$ and inputs (v_1, v_2) can be obtained as follows

$$\begin{aligned} v_1 &= RI_1 + u_1 \\ &= RI_1 + w_2 - w_1 \\ &= RI_1 + k_1\left(\phi_{bd} - \frac{\phi_1+\phi_2}{2}\right) - k_2\theta - k_3\dot{\theta} - k_4\frac{\phi_2-\phi_1}{2} \end{aligned}$$

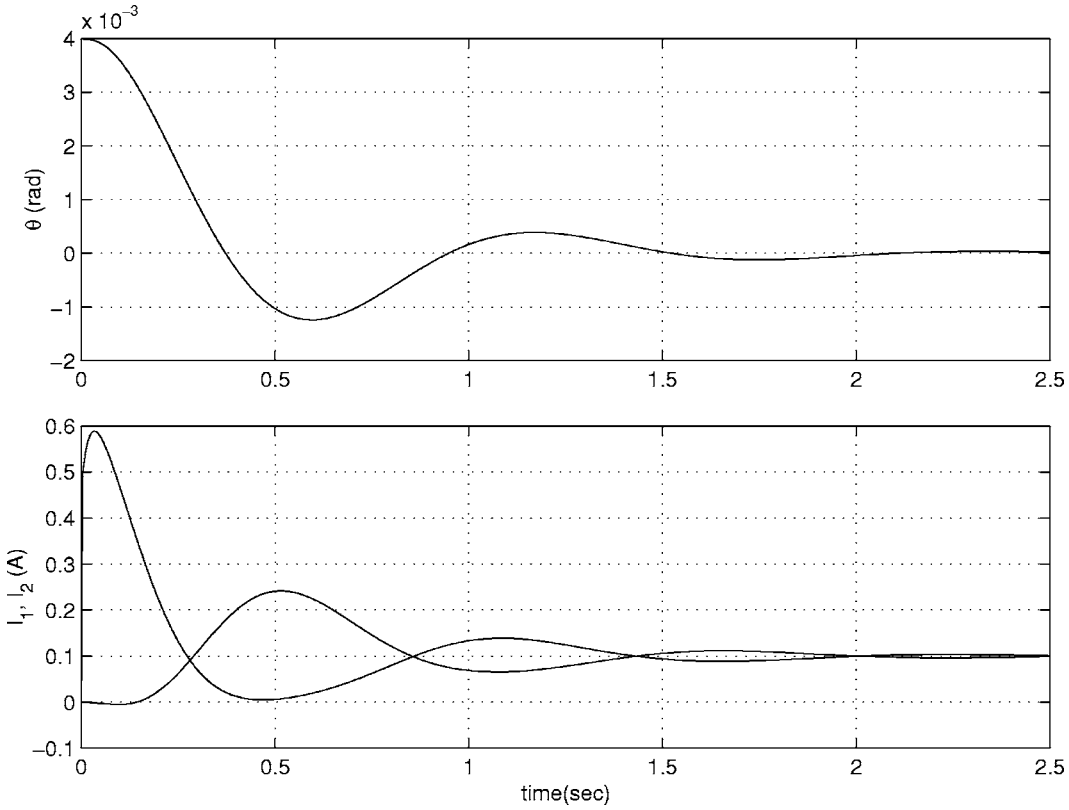

Fig. 11 Simulation: time responses of θ, I_1, and I_2 of the exact system

$$= -k_2\theta - k_3\dot{\theta} + \left(R + \frac{(k_4 - k_1)g_0 L_0}{2(g_0 + \theta)}\right) I_1 - \frac{(k_4 + k_1)g_0 L_0}{2(g_0 - \theta)} I_2 + k_1 \phi_{bd}, \tag{36}$$

and

$$\begin{aligned} v_2 &= RI_2 + u_2 \\ &= RI_2 + w_2 + w_1 \\ &= RI_2 + k_1\left(\phi_{bd} - \frac{\phi_1 + \phi_2}{2}\right) + k_2\theta + k_3\dot{\theta} + k_4\frac{\phi_2 - \phi_1}{2} \\ &= k_2\theta + k_3\dot{\theta} - \frac{(k_4 + k_1)g_0 L_0}{2(g_0 + \theta)} I_1 + \left(R + \frac{(k_4 - k_1)g_0 L_0}{2(g_0 - \theta)}\right) I_2 + k_1\phi_{bd}. \end{aligned} \tag{37}$$

To satisfy the voltage bound, we may assign a bound to each item RI_1, RI_2, w_1, and w_2. The bounds on RI_1 and RI_2 can be computed from the bounds on the currents, $|I_1|, |I_2| \leq I_M$. Let the bounds on w_1 and w_2 be w_{1M} and w_{2M}, and let the maximal value of the voltage supply be v_M, then we need to choose w_{1M} and w_{2M} such that $w_{1M} + w_{2M} + RI_M \leq v_M$.

The bias flux ϕ_{bd} corresponds to a bias current $I_b = \phi_{bd}/L_0$ at steady state. The bounds on the currents impose a bound on the flux as $|\phi_1|, |\phi_2| \leq L_0 I_M/2$, so we need to restrict ϕ such that $|\phi| \leq L_0(I_M/2 - I_b)$.

In summary, for (34), we need to consider the following state and input constraints,

$$|\theta| \leq \theta_M, \quad |\phi| \leq L_0(I_M - I_b), \quad |w_1| \leq w_{1M}.$$

In order to design the control law (35), we may set the objective as finding the invariant ellipsoid $\mathcal{E}(P)$ that contains $\alpha[1 \;\; 0 \;\; 0]^T$ with α maximized. This will result in the largest initial displacement of the beam that can be brought back to the balance position. This objective can be easily transformed into the optimization problem (6), which can be solved efficiently.

As to the design of the control law (33), suppose that the initial ϕ_b is 0; then $|\phi_{bd} - \phi_b| \leq \phi_{bd}$ for all time. The constraint on w_2 can be easily satisfied by choosing k such that $k\phi_{bd} \leq w_{1M}$.

Example 3. Consider the same balance beam test rig as in Example 1. The additional parameters in the circuit systems are

$$R = 0.7\ \Omega, \quad L_0 = 4.9060 \times 10^{-4} H.$$

We used a PWM (pulse width modulated) power amplifier to provide a desired voltage. The voltage bound is $v_M = 15$ V. We set $I_M = 2$ A, $w_{1M} = 10$ *V*, and $w_{2M} = 3.6$ V. We choose $\phi_{bd} = 0.1L_0$ and take $\beta = 4$ to ensure some stability margin. The optimal value of α is 0.0037 and the control law is

$$w_1 = 10\,\mathrm{sat}(-38.6\theta - 4.6\dot{\theta} - 1353.9\phi), \quad w_2 = 50(\phi_{bd} - \phi).$$

For the closed-loop system (34) and (35), the point $(\theta, \dot{\theta}, \phi) = (0.0037, 0, 0)$ is in the resulting invariant ellipsoid $\mathcal{E}(P)$. Since $\mathcal{E}(P)$ could be conservative as an estimation of the stability region, we tried an initial state $(\theta, \dot{\theta}, \phi) = (0.003\,99, 0, 0)$ and simulation confirms that this point is still in the stability region. Figure 11 plots the simulation results with initial conditions $(\theta, \dot{\theta}, \phi) = (0.003\,99, 0, 0)$ and $\phi_b = 0$.

From the simulation result, it is expected that the controller can bring the beam to the balance position from initially almost touching one of the electromagnets. However, we did not do this successfully at the first trials on the experiment. Actually, we were unable to manipulate the beam into a position that could be stabilized. To find out the reason, we did some simulation by adding some disturbances to the voltage supply. Instead of letting $v_1 = RI_1 + w_2 - w_1$ and $v_2 = RI_2 + w_2 + w_1$ as in (36) and (37), we output

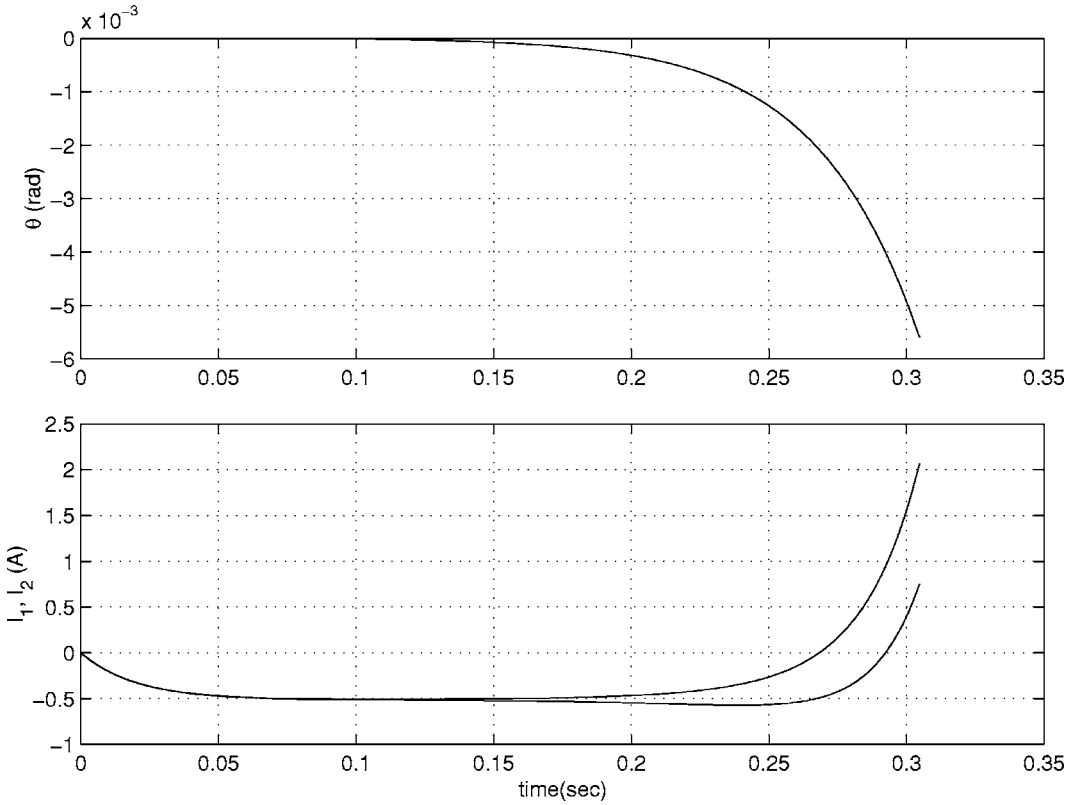

Fig. 12 Simulation: unstable responses under actuator uncertainties

$$v_1 = RI_1 + w_2 - w_1 + v_{10}, \quad v_2 = RI_2 + w_2 + w_1 + v_{20}$$

from the controller. Figure 12 plots the simulation results with $v_{10}=-0.02$ V, $v_{20}=-0.01$ V and initial conditions $(\theta, \dot{\theta}, \phi, \phi_b) = (0,0,0,0)$. Clearly, the time responses are diverging and indicating instability.

The simulation results thus show that the control system is very sensitive to voltage drifts. The reason is that, in the control law (36) and (37), the term $k\phi_{bd}$ is very small. In the case $k=50$ and $I_b=0.1$, $k\phi_{bd}=0.0025$. A small drift of the voltage would result in a large drift of the effective ϕ_{bd}. Recognizing this, we checked the drift of the voltages and made some correction. The behavior of the test rig was indeed improved. The first plot in Fig. 13 is the time response of the angle plotted from experimental data. The second and the third plots in Fig. 13 are the currents I_1 and I_2. The beam went back to the balance position after pushing to the electromagnets and releasing. However, the currents, which should be around 0.1 A, were actually about 0.25 A in the steady state. The deviation of the currents from the theoretical value is caused by the positive voltage drifts. In fact, it is impossible to eliminate the voltage drifts completely.

Since we used a PWM power amplifier, the currents are subject to severe disturbances. We can see from the plots in Fig. 13 that the disturbances are of very high frequency and large amplitudes as compared with the average values. However, these large disturbances do not seem to have a large influence on the performance of the test rig. This is because the mechanical system acts as a low-pass filter. The main disadvantage of the voltage mode is that it is very sensitive to actuator uncertainties. This is possibly caused by the PWM power amplifier.

4 Performance Improvement

We presented three approaches for stabilizing magnetic bearing systems in Sec. 3. From our experience with the experimental test rig, the exact linearization approach under the current mode exhibits the best properties in several important aspects, including the large stability region, robustness, and disturbance rejection. For other magnetic bearing systems, different control strategies may be more effective. In this section, we will focus on improving the transient performance for the exact linearized system under the current mode.

In Sec. 2.3 we present an approach to improving the transient performance by solving the optimization problem (8). Two controllers can be constructed from the optimal solution:

$$u = \text{sat}(Fx) \tag{38}$$

and

$$u = -\text{sat}(kB^T Px). \tag{39}$$

The gain k needs to be adjusted for the best results. In what follows, we use an example to illustrate the effectiveness of the design technique.

Example 4. Consider again the balance beam test rig. In solving the optimization problem (8), we choose $\ell=1$ and $x_1=\begin{bmatrix} 0.003 \\ 0 \end{bmatrix}$. The state constraint is represented by $\mathcal{L}(G)$ with $G=[1/0.004 \quad 0]$. Here is the optimal solution for the case $I_b=0.1$ A:

$$\beta = 15.1640, \quad F = [249.9996 \quad 28.8509],$$

$$P = \begin{bmatrix} 1.1111 & 0.0641 \\ 0.0641 & 0.0085 \end{bmatrix} \times 10^5.$$

Based on this solution, we obtained two controllers

$$I = 0.9\,\text{sat}(Fx) = 0.9\,\text{sat}(249.9996\theta + 28.8509\dot{\theta}), \tag{40}$$

and

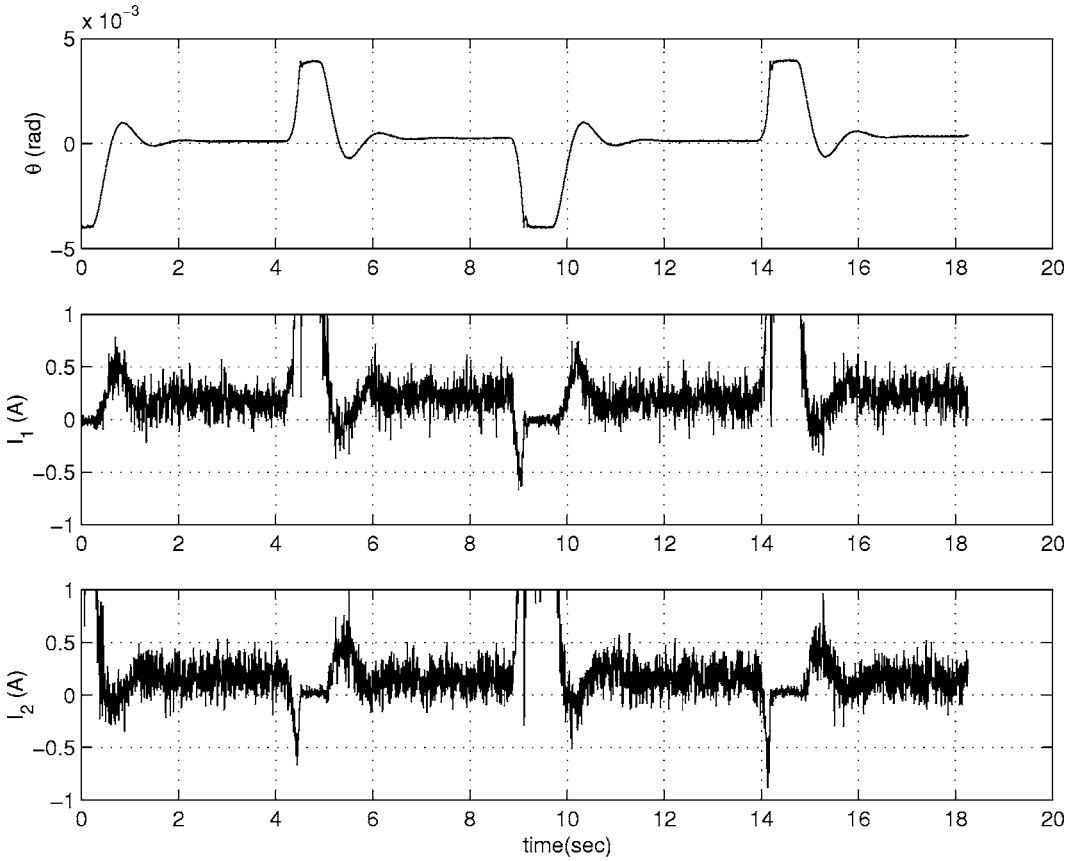

Fig. 13 Experimental results: stable time responses of θ, I_1, and I_2

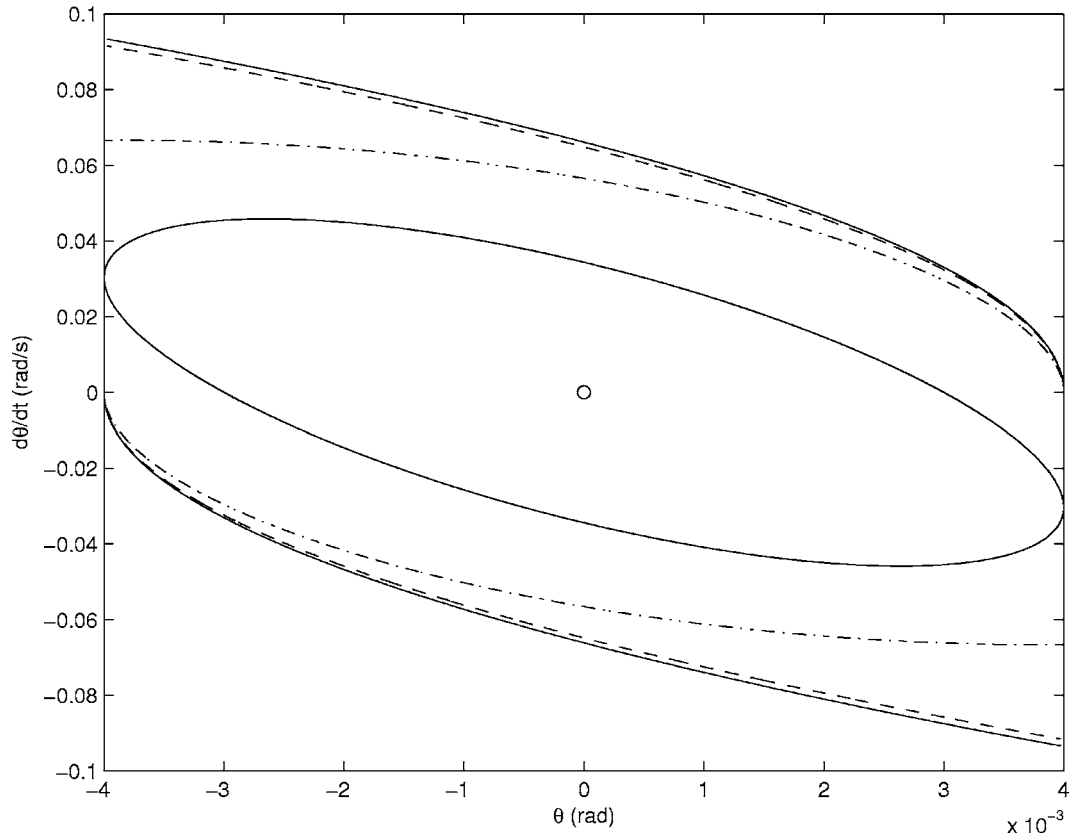

Fig. 14 Stability regions under different feedback laws: I_b=0.1

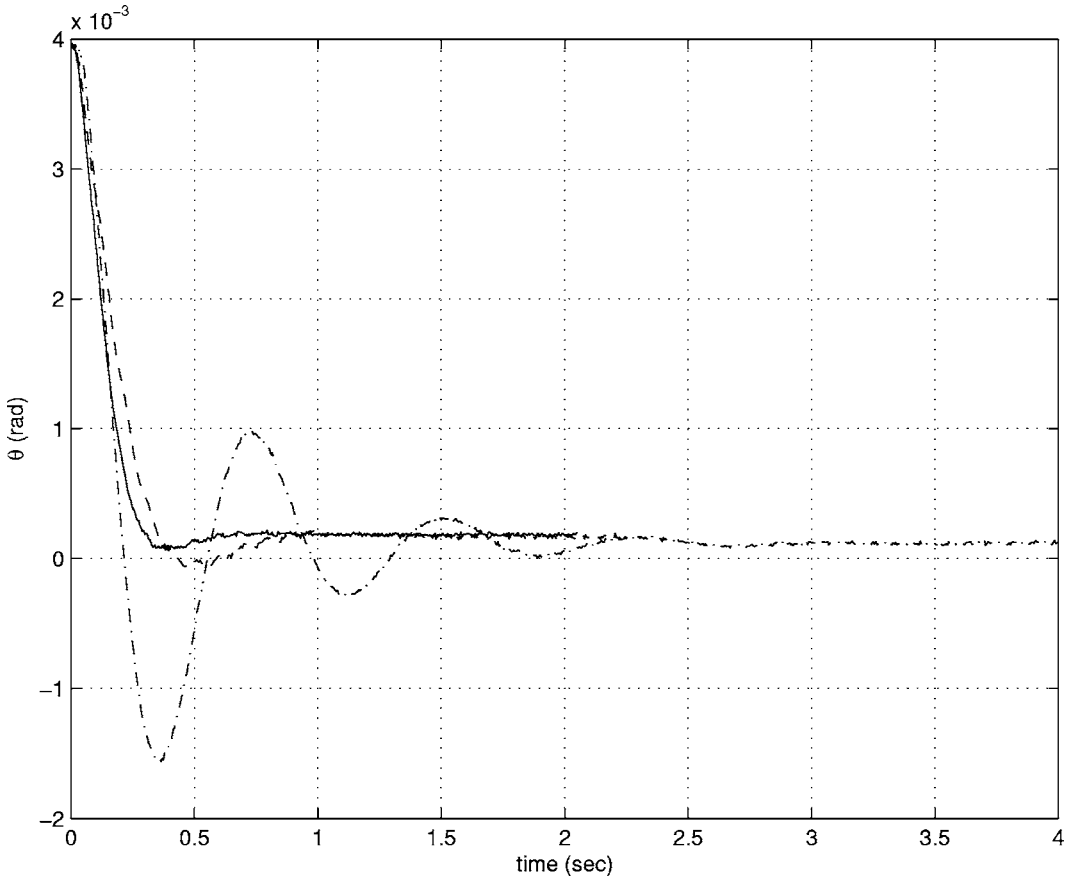

Fig. 15 Experimental results: time responses of θ under control laws (23), (40), and (41)

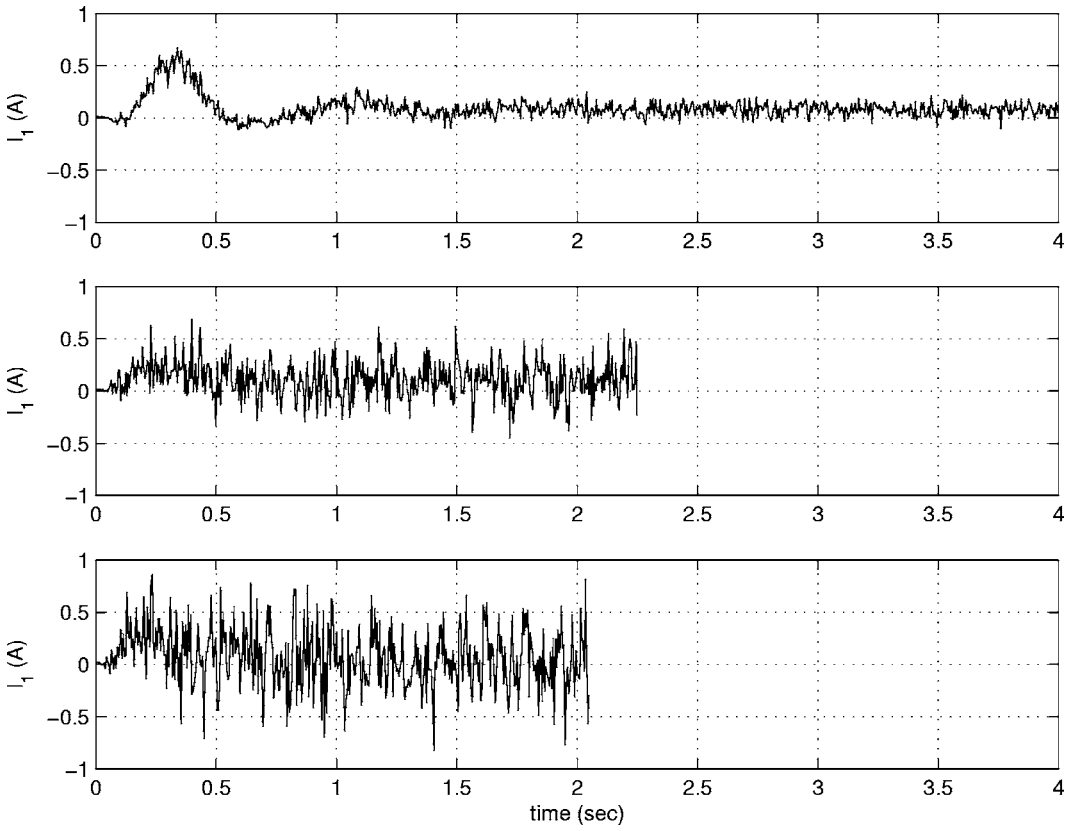

Fig. 16 Experimental results: time responses of I_1 under control laws (23), (40), and (41)

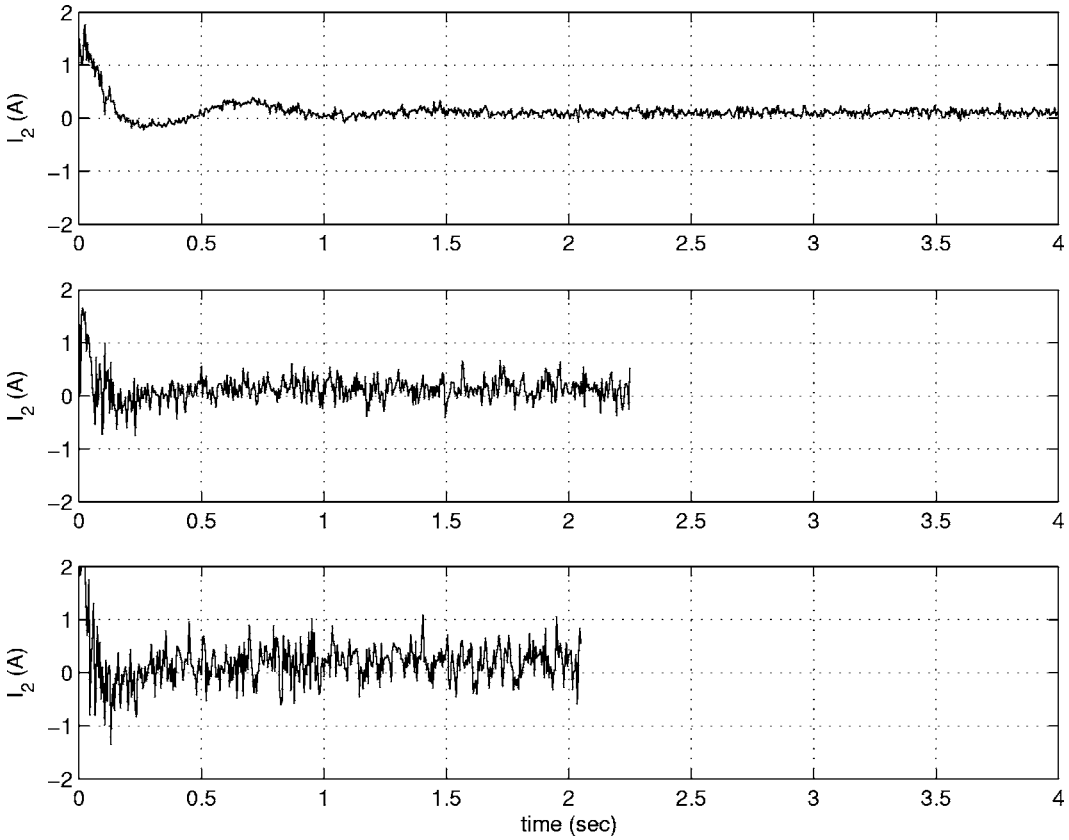

Fig. 17 Experimental result: time responses of I_2 under control laws (23), (40), and (41)

$$I = 0.9\ \mathrm{sat}(kB^{\mathrm{T}}Px) = 0.9\ \mathrm{sat}(336.9784\theta + 44.4445\dot{\theta}). \quad (41)$$

The boundaries of the stability regions under these two controllers are plotted in Fig. 14, where the dashed curves correspond to (40) and the solid curves correspond to (41). (The solid boundary and the dashed boundary are very close.) The ellipsoid is the estimate of the stability region $\mathcal{E}(P)$. For comparison, we also plot the boundary of the stability region under the controller (23) in dash-dotted curves. We see that the two controllers (40) and (41) not only produce better performances, but also larger stability regions. This result is somewhat unexpected, but gives some indication about how saturation may complicate the analysis problems. Experimental results show that the performance of the balance beam is much improved by using the controllers (40) and (41). Figure 15 compares the time responses of the angle under these controllers and that under the controller (23), where the dash-dotted curve corresponds to (23), the dashed curve to (40), and the solid curve to (41). The time response under (23) is plotted from $t=0$ to $t=4$, while the time responses under (40) and (41) are plotted over shorter periods of time. This is because the steady state was reached much earlier under (40) and (41).

Figures 16 and 17 plot the time responses of the currents. In each figure, the first plot is the current under the controller (23), the second plot under (40), and the third plot under (41). In each plot, the average value of the currents are about 0.1 A in the steady state. But the variation is larger under the controllers (40) and (41). The reason is that, in these two controllers, the coefficients of $\dot{\theta}$ are larger than that in (23) and the measurement of the rotational velocity is subject to a larger disturbance than the measurement of the angle. If we increase the gain k in the controller (41), this disturbance will be further amplified and result in larger variations of the currents. If the currents exceed the saturation level, then the performance and stability of the system cannot be guaranteed.

5 Conclusions

In this paper we developed a systematic control design approach for magnetic bearing systems that are subject to both input and state constraints. We extended some of our recently developed tools to design controllers for the purposes of enlarging the stability region and improving the transient performance. We investigated three design approaches through three different linearization methods and compared the stability performances under these approaches. The analysis and design results were verified on a balance beam test rig.

References

[1] Allaire, P. E., Maslen, E. H., Humphris, R. R., Knospe, C. R., and Lewis, D. W., 1994, "Magnetic Bearings," *CRC Handbook of Lubrication and Tribology*, edited by R. Booser, CRC Press, Vol. 3, pp. 577–600.

[2] Allaire, P. E., Hilton, E., Baloh, M., Maslen, E., Bearnson, G., Noh, D., Khanwilkar, P., and Olsen, D., 1998, "Performance of Continuous Flow Ventricular Assist Device (CFVADIII): Magnetic Bearing Design, Construction, and Testing," Artif. Organs, **22**, pp. 475–480.

[3] Antila, M., Lantto, E., Saari, J., Esa, H., Lindgren, O., and Sily, K., 1996, "Design of Water Treatment Compressors Equipped With Active Magnetic Bearings," *Proc. 5th International Symposium on Magnetic Bearings*, Kanazawa, Japan, pp. 389–394.

[4] Kyung, J. H., and Lee, C. W., 2002, "Controller Design for a Magnetically Suspended Milling Spindle Based on Chatter Stability Analysis," *Proc. 8th International Symposium on Magnetic Bearings*, Mito, Japan, pp. 327–332.

[5] Li, G., Lin, Z., Allaire, P. E., Huang, B., Jiang, W., Zorzi, E. S., and Bartlett, R. O., 2001, "Stabilization of a High Speed Rotor with Active Magnetic Bearings by a Piecewise H-Synthesis Controller," *Proc. 6th International Symposium on Magnetic Suspension Technology*.

[6] Maslen, E. H., Bearnson, G. B., Allaire, P. E., Flack, R. D., Baloh, M., Hilton, E., Noh, D., Olson, D., Khanwilkar, P. S., and Long, J. D. 1998, "Feedback Control Applications in Artificial Hearts," IEEE Control Syst. Mag., **18**, pp. 26–34.

[7] Takahata, R., and Ueiama, H., 1996, "Development of Flywheel Energy Storage System With Hybrid AMB-SMB," *Proc. 5th International Symposium on Magnetic Bearing*.

[8] Hu, T., Lin, Z., Huang, B., and Allarie, P. E., 2001, "On Minimum Current

Biasing and Control For a Balanced Beam Suspended on Magnetic Bearings," *Proc. 6th International Symposium on Magnetic Suspension Technology*, Turin, Italy, pp. 410–415.
[9] Baloh, M., 2001, "Time Varying Feedback Linearization of Magnetic Bearing Actuator," Ph.D. dissertation, University of Virginia, 2001.
[10] Levine, J., Lottin, J., and Ponsart, J-C., 1996, "A Nonlinear Approach to the Control of Magnetic Bearings," IEEE Trans. Control Syst. Technol., **4**, pp. 524–544.
[11] Charara, A., De Miras, J., and Caron, B., 1996, "Nonlinear Control of a Magnetic Levitation System Without Premagnetization," IEEE Trans. Control Syst. Technol., **4**, pp. 513–523.
[12] Li, L., 1999, "Linearization of Feedback Actuators by Constant Current Sum, Constant Voltage Sum and Constant Flux Sum," IEEE Trans. Magn., **35**, pp. 528–535.
[13] Malsen, E. H., Hermann, P., and Scott, M., 1989, "Practical Limits to the Performance of Magnetic Bearings: Peak Force, Slew Rate and Displacement Sensitivity," ASME J. Tribol., **111**, pp. 331–336.
[14] Tsiotras, P., and Velenis, E., 2000, "Low-Bias Control of AMB's Subject to Saturation Constraints," *IEEE International Conf. on Control and Application*, Anchorage, AK, pp. 138–143.
[15] Yang, C., 1997, "Control of Magnetic Bearings With Low Bias Flux and Saturating Voltage," MS thesis, University of Virginia.
[16] Hu, T., and Lin, Z., 2001, *Control Systems with Actuator Saturation: Analysis and Design*, Birkhäuser, Boston.
[17] Hu, T., and Lin, Z., 2000, "On Enlarging the Basin of Attraction for Linear Systems Under Saturated Linear Feedback," Syst. Control Lett., **40**, pp. 59–69.
[18] Hu, T., Lin, Z., and Chen, B. M., 2002, "An Analysis and Design Method for Linear Systems Subject to Actuator Saturation and Disturbance," Automatica, **38**, pp. 351–359.
[19] Li, L., and Mao, J., 1999, "Feedback Linearization of Magnetic Bearing Actuators for Uniform Upward Bound of Force Slew Rate," IEE Proc.: Electr. Power Appl., **146**, pp. 378–382.
[20] Boyd, S., El Ghaoui, L., Feron, E., and Balakrishnan, V., 1994, *Linear Matrix Inequalities in Systems and Control Theory*, SIAM Studies in Appl. Mathematics, Philadelphia.
[21] Kothare, M. V., Balakrishnan, V., and Morari, M., 1996, "Robust Constrained Model Predictive Control Using Linear Matrix Inequalities," Automatica, **32**, pp. 1361–1379.